TRANSPORT OF FINE SANDS BY CURRENTS AND WAVES. II

By Leo C. Van Rijn[1] and Fred J. Havinga[2]

ABSTRACT: The transport process of fine sand with a median diameter of about 100 μm in combined current and wave conditions in a laboratory basin was studied. Irregular waves with a single-topped spectrum and peak period of 2.5 s were generated. The significant wave height was varied from 0.07 m to 0.14 m. The water depth was about 0.4 m in all tests. The depth-mean current velocities were varied from 0.1 m/s to 0.3 m/s. The angles between the wave and current directions were 60°, 90°, and 120°. Instantaneous fluid velocities were measured by an acoustical probe and an electromagnetic probe. The acoustical probe was also used to measure the instantaneous sand concentrations. Time-averaged and bed-averaged concentrations were measured by a pump sampler. Current-related and wave-related transport rates were determined by decomposing, multiplying, and time-averaging instantaneous signals. The current-related transport rate in the main current direction was found to be largest when the waves were propagating normal to the current. High-frequency wave-related transport rates were found to be directed onshore because of the wave asymmetry effect. Low-frequency wave-related transport rates were found to be directed offshore because of the bound long waves.

INTRODUCTION

The transport of fine sand under waves in combination with following and opposing currents (as present in flume conditions) was studied by Van Rijn et al. (1993). The influence of the current direction on the concentration profile and transport rate was found to be rather small. To extend this information to the general case of sand transport in waves and currents making an arbitrary angle, mobile bed experiments were carried out in a large basin at Delft Hydraulics. This study was a joint project of Delft Hydraulics, Delft University of Technology, Rijkswaterstaat of the Dutch Ministry of Public Works, and the MAST-program of the European Communities.

IDENTIFICATION OF TRANSPORT PROCESSES

To demonstrate the relative importance of the various transport processes in coastal seas, the instantaneous velocity and concentration values at a certain elevation above the bed are decomposed as follows [also see Van Rijn (1993)]:

$$U = u + \tilde{U}_s + \tilde{U}_L; \quad V = v + \tilde{V}_s + \tilde{V}_L; \quad C = c + \tilde{C}_s + \tilde{C}_L \tag{1-3}$$

in which U, V = instantaneous cross shore and longshore velocity at height z above the bed; C = instantaneous sand concentration at height z above the bed; u, v = time-averaged velocities; c = time-averaged concentration; $\tilde{U}_s$, $\tilde{V}_s$ = high-frequency velocity oscillations; $\tilde{U}_L$, $\tilde{V}_L$ = low-frequency velocity oscillations; $\tilde{C}_s$ = high-frequency concentration oscillation; and $\tilde{C}_L$ = low frequency concentration oscillation.

High-frequency velocity oscillations are generated by turbulent eddies and wind waves. Low-frequency oscillations are related to macroscale turbulence and to (free and bound) long waves. The net transport rate at a perpendicular level above the bed can be obtained by time-averaging the instantaneous data (indicated by an overbar). This yields in the cross-shore direction (for example)

$$q_{net} = \overline{UC} = uc + \overline{\tilde{U}_s\tilde{C}_s} + \overline{\tilde{U}_s\tilde{C}_L} + \overline{\tilde{U}_L\tilde{C}_s} + \overline{\tilde{U}_L\tilde{C}_L} \tag{4}$$

The uc component is termed the current-related flux, whereas the $\overline{\tilde{U}\tilde{C}}$ components are termed the wave-related fluxes. Similar expressions can be obtained for the longshore direction. The depth-integrated transport rates can be obtained by the integration of (4) over the water depth.

The transport processes associated with the various terms of (4) can be described as follows:

[1]Sr. Engr., Delft Hydraulics, P.O. Box 152, Emmeloord, The Netherlands.
[2]Grad. Student, Fac. of Civ. Engrg., Hydr. Sect., Delft Univ. of Technol., P.O. Box 5048, Delft, The Netherlands.

Note. Discussion open until September 1, 1995. Separate discussions should be submitted for the individual papers in this symposium. To extend the closing date one month, a written request must be filed with the ASCE Manager of Journals. The manuscript for this paper was submitted for review and possible publication on September 27, 1993. This paper is part of the ***Journal of Waterway, Port, Coastal, and Ocean Engineering***, Vol. 121, No. 2, March/April, 1995. ©ASCE, ISSN 0733-950X/95/0002-0123–0133/$2.00 + $.25 per page. Paper No. 7060.

- The generation of a quasisteady mean current near the bed will result in a quasisteady transport component (uc).
- The generation of high-frequency asymmetric waves in shallow water will result in relatively large peak velocities under the wave crests and relatively small peak velocities under the wave troughs, which may result in a net forward or backward transport component ($\tilde{U}_s\tilde{C}_s$), depending on bed conditions (flat or rippled bed).
- The generation of low-frequency bound long waves related to a mean water surface increase under low-amplitude waves and a mean water surface decrease under high-amplitude waves may result in a net backward transport component ($\tilde{U}_L\tilde{C}_L$) because sand concentrations will be high under high waves and low under low waves ($\tilde{U}_L$ and $\tilde{C}_L$ are out of phase).
- The flux terms related to the interaction of high- and low-frequency components will be approximately zero because $\tilde{U}_s$ and $\tilde{C}_L$ and $\tilde{U}_L$ and $\tilde{C}_s$ are uncorelated.

In this study, attention is focused primarily on the uc-, $\overline{\tilde{U}_s\tilde{C}_s}$-, and $\overline{\tilde{U}_L\tilde{C}_L}$-flux components.

EXPERIMENTAL SETUP

The experiments were carried out in a wave-current basin, as shown in Fig. 1. Irregular waves were generated by a directional wave generator. The wave spectrum (JONSWAP form) was single-topped with a peak frequency of 0.4 Hz. The water depth was about 0.4 m in all tests. Three different wave conditions were used with significant wave heights of 0.07 m, 0.1 m, and 0.14 m for each wave direction. In all, three wave directions were considered—60°, 90°, and 120° (angle between wave orthogonal and current direction, see Fig. 1). A pump system was used to generate a current. Guiding boards were used to confine the current in a channel (width = 4 m) with a movable bed consisting of fine sand (d_{50} = 100 μm, d_{90} = 130 μm). The guiding boards were placed normal to the wave crests in all experiments. Three different current velocities (0.1, 0.2, and 0.3 m/s) were generated by varying the pump discharge. The velocity distribution across the channel was found to be almost uniform (current alone). The vertical distribution of the velocity in the middle of the channel was perfectly logarithmic in all tests (current alone). The vertical distribution of the turbulence intensity was found to be in good agreement with

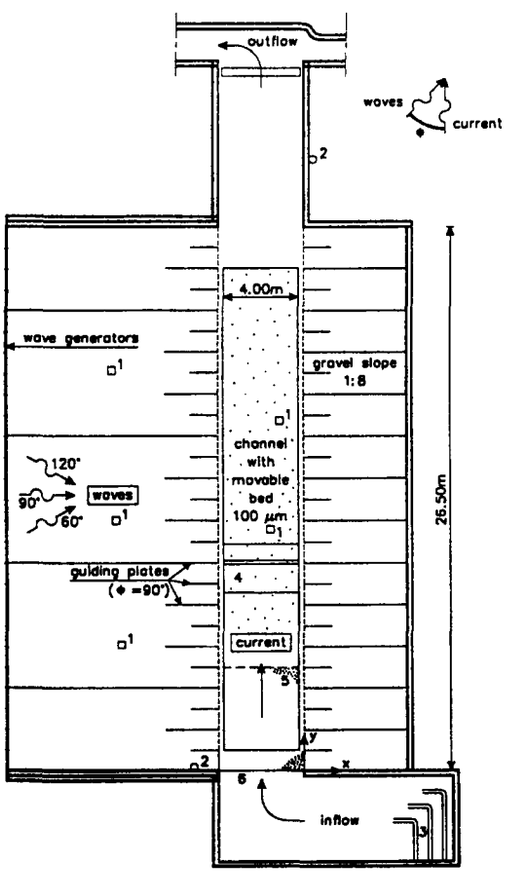

FIG. 1. Plan View of Experimental Setup (1 = Wave Height Meter, 2 = Water Level Gauge, 3 = Inflow Pipes, 4 = Measurement Carriage, 5 = Gravel Bed)

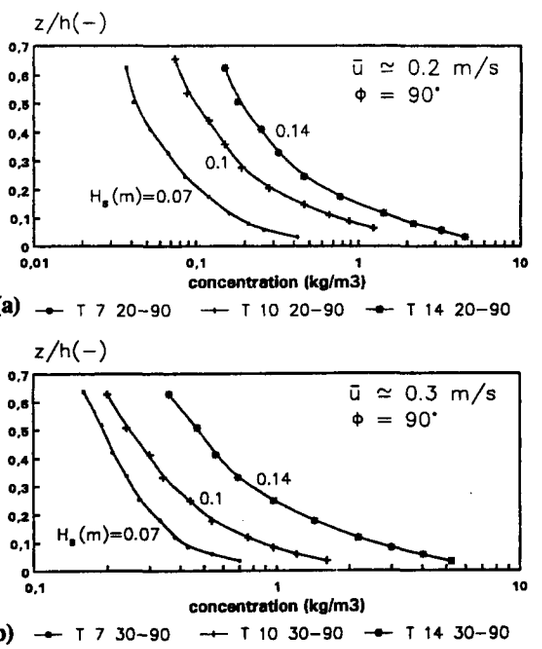

FIG. 2. Influence of Wave Height on Concentration Profile

values reported in the literature (current alone). Details were presented by Havinga (1992). Based on this, it was concluded that the effect of the guiding boards on the current and, hence, on the transport process was negligible.

The water entering the channel had no initial sediment load. Consequently, the concentration profiles were generated by the erosion of sediment particles from the bed. To provide enough length for establishing equilibrium concentration profiles, the measuring section was situated at a distance of about 30 times the water depth from the channel entrance.

Measurements of wave height, velocity, and sediment concentration were performed from a carriage moving over rails above the channel. Water-level variations were measured by a resistance probe near the location at which the concentrations and velocities were measured (measuring period = 30 min). Characteristic wave parameters were computed from the data records and stored in a computer.

Instantaneous sediment concentrations were measured by an acoustic probe (AZTM); time-averaged sediment concentrations were determined from water-sediment samples using a pump sampler. The pump sampler consisted of an array of 10 intake tubes of 3 mm internal diameter connected to the pumps by plastic hoses. The lowest intake tube was placed at about 0.01 m above the crest level of the bed forms. The intake openings were placed in a direction transverse to the plane of orbital motion. The intake velocity was about 1 m/s, satisfying sampling requirements. The 10-L samples were collected in calibrated buckets.

Instantaneous velocities were measured using an electromagnetic velocity meter (EMS) with a measuring level at about 3 mm below the probe and the acoustic probe (AZTM). The velocities were measured at the same elevations above the mean bed as those of the concentrations starting at the lowest point and working upward. A time-averaging period of 256 s (approximately 100 waves) was applied. Details of instrument characteristics are given by Havinga (1992).

Space-averaging over the bed-form length was performed by moving the sediment concentration and fluid velocity forward and backward over a certain longitudinal distance by using an oscillating carriage above the channel. The velocity of the moving carriage (approximately 0.01 m/s) was small compared with the fluid velocity, and large when compared with the bed-form migration velocity. The error in the time-averaged velocity was less than 0.00125 m/s in the tests. Preliminary tests showed that a space-averaging distance of 0.6 m (approximately 5 ripple lengths) was large enough to give reproducible results.

The test program and basic hydraulic data are given in Table 1. The test code refers to the approximate wave height (cm), the approximate current velocity (cm/s), and the wave direction (degrees). Detailed velocity and concentration data are presented by Havinga (1992).

TABLE 1. Basic Hydraulic Data

Test code (1)	Water depth h (m) (2)	Wave height H_s (m) (3)	Peak period T_p (4)	Wave-current angle ϕ (degree) (5)	Current velocity $\bar{u}$ (m/s) (6)	Ripple height Δ (m) (7)	Ripple length λ (m) (8)
T7 0 90	0.41	0.067	2.28	—	0	0.010	0.059
T7 10 90	0.43	0.068	2.24	90	0.104	0.008	0.102
T7 20 90	0.42	0.076	2.16	90	0.246	0.007	0.073
T7 30 90	0.42	0.076	2.16	90	0.311	0.009	0.094
T10 0 90	0.41	0.095	2.28	—	0	0.010	0.060
T10 10 90	0.43	0.093	2.24	90	0.117	0.007	0.095
T10 20 90	0.42	0.105	2.16	90	0.246	0.007	0.084
T10 30 90	0.42	0.099	2.13	90	0.313	0.008	0.075
T14 0 90	0.41	0.133	2.28	—	0	0.008	0.059
T14 10 90	0.42	0.133	2.24	90	0.131	0.007	0.097
T14 20 90	0.42	0.139	2.28	90	0.256	0.009	0.097
T14 30 90	0.42	0.137	2.19	90	0.317	0.009	0.091
T7 10 60	0.40	0.066	2.34	60	0.120	0.006	0.073
T7 20 60	0.41	0.072	2.34	60	0.241	0.013	0.102
T7 30 60	0.41	0.072	2.28	60	0.299	0.011	0.090
T10 10 60	0.41	0.094	2.31	60	0.128	0.008	0.084
T10 20 60	0.41	0.097	2.34	60	0.241	0.013	0.100
T10 30 60	0.41	0.095	2.21	60	0.306	0.011	0.088
T14 10 60	0.40	0.128	2.34	60	0.122	0.007	0.092
T14 20 60	0.42	0.131	2.30	60	0.235	0.010	0.086
T14 30 60	0.42	0.135	2.28	60	0.297	0.014	0.111
T7 20 120	0.41	0.072	2.28	120	0.239	0.008	0.064
T10 10 120	0.43	0.112	2.24	120	0.123	0.007	0.067
T10 20 120	0.43	0.113	2.28	120	0.247	0.008	0.079
T10 30 120	0.42	0.122	2.28	120	0.299	0.013	0.105
T14 10 120	0.42	0.130	2.28	120	0.126	0.008	0.079
T14 20 120	0.43	0.127	2.28	120	0.263	0.008	0.074
T14 30 120	0.42	0.131	2.28	120	0.321	0.010	0.096

EXPERIMENTAL RESULTS

Time- and Bed-Averaged Concentration

Fig. 2 shows the influence of the wave height on the concentration profiles for currents of 0.2 and 0.3 m/s and a wave-current angle of 90°. An increase of the wave height results is an increase of the concentrations over the full depth.

Fig. 3 shows the influence of the current velocity on the concentration profile for a wave height of 0.07 and 0.1 m and a wave-current angle of 90°. The bed level $z = 0$ represents the mean (space-averaged) bed level. As can be observed, the concentrations outside the near-bed layer show a considerable increase for increasing current velocities because of the mixing effect. However, the concentrations in the near-bed layer are not noticeably affected by the current velocity increase. The near-bed concentrations are almost completely determined by the wave conditions.

Fig. 4 shows the influence of the wave-current angle for current velocities of 0.1 and 0.2 m/s and a wave height of 0.14 m. Wave propagation normal to the current direction yields the largest concentrations (in all tests). The differences in concentrations for angles of 60° and 120° are not considered significant given the concentration variations observed during repetition tests.

Time- and Bed-Averaged Fluid Velocities

The measured velocity profiles show a clear influence of the waves on the vertical distribution of velocities. The presence of waves caused a decrease (maximum 20%) of the velocities in the near-bed layer ($z/h < 0.2$) and an increase of the velocities (maximum 20%) in the outer layer. Similar results were observed earlier by Kemp and Simons (1982, 1983) and by Van Rijn et al. (1993). In the present experiments the near-bed velocities were smallest for a wave-current angle of 90°, as shown in Fig. 5. The velocities have been made dimensionless with the depth-averaged velocity.

Ripple and Roughness Characteristics

Based on visual observations, the following ripple configurations were defined (see Fig. 6):

- Two-dimensional ripples are regular ripples (straight crests) in the wave direction.
- 2.5-dimensional ripples are wave-related ripples with curved crests.
- Three-dimensional ripples are regular ripples in the wave and current directions (honeycomb pattern).

Two-dimensional ripples were observed in conditions with waves alone (no current). The ripple crests became somewhat wavy in the case of relatively high waves in combination with a weak

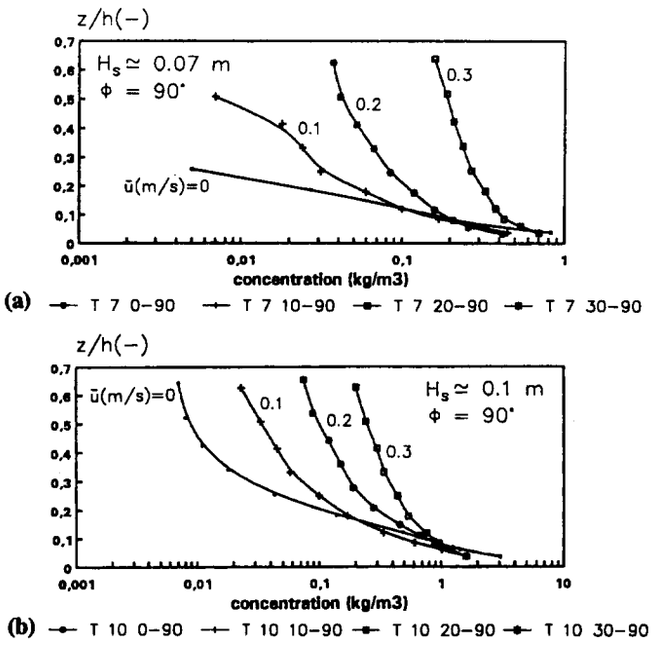

FIG. 3. Influence of Current Velocity on Concentration Profile

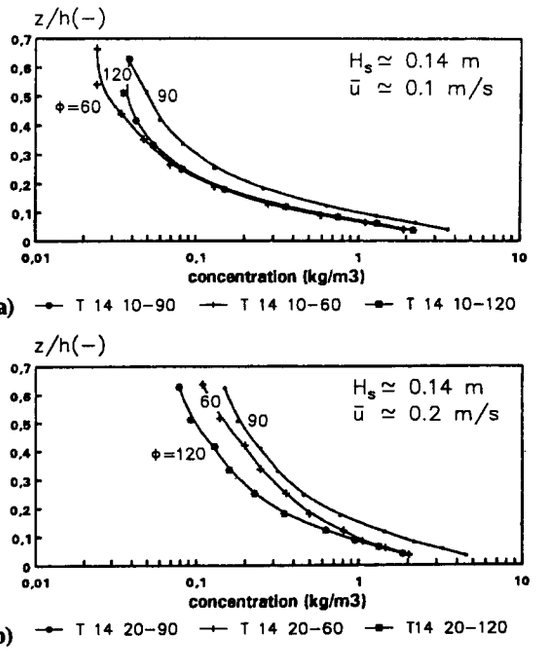

FIG. 4. Influence of Wave-Current Angle on Concentration Profile

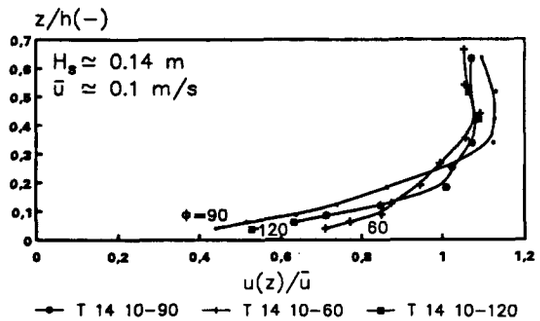

FIG. 5. Influence of Wave-Current Angle on Velocity Profile

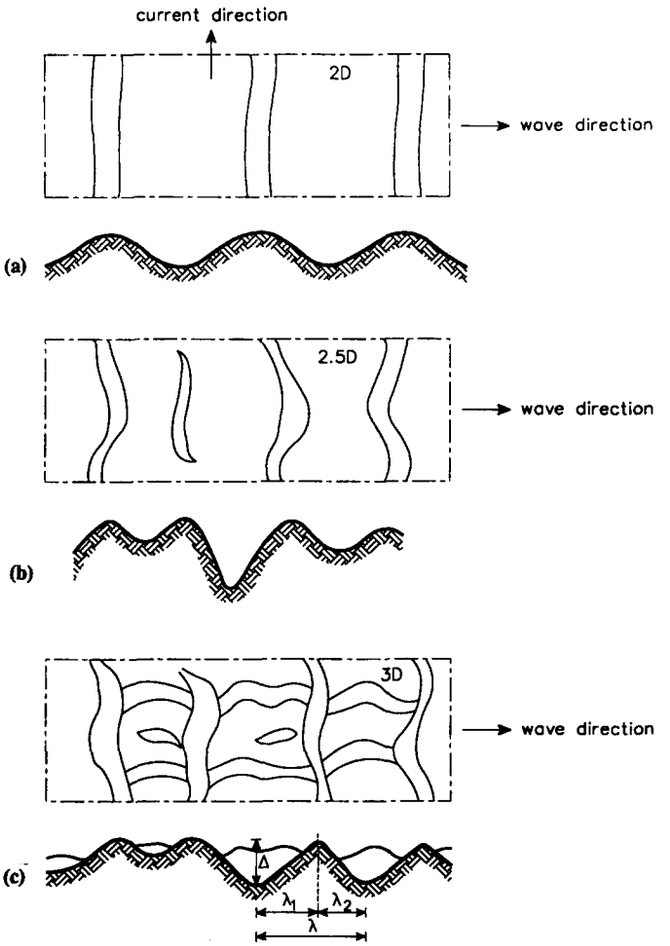

FIG. 6. Ripple Configurations

current. The ripples became three-dimensional (honeycomb pattern with two distinct directions) when a relatively strong current was generated. Bed-level surroundings were used to determine the ripple height and length in the wave and in the current direction (Δ_c, Δ_w, λ_c, λ_w), the ripple steepness (Δ/λ), and the ripple asymmetry (λ_1, λ_2) (see Fig. 6). The mean ripple data are presented in Table 1. Ripples generated in the wave direction were reasonably symmetric with λ_1/λ_2-values in the range of 0.85 to 1.3. The ripples in the current direction were asymmetric with values in the range of 1.1 to 1.6. These latter asymmetrical values were found independent of the relative strength of the current velocity and the peak orbital velocity near the bed ($\bar{u}/\hat{U}_\delta$). The ripple heights in the wave direction and those in the current direction were about equal ($\Delta_w = \Delta_c$). The relative ripple height ($\Delta/\hat{A}_\delta$) and ripple length ($\lambda/\hat{A}_\delta$) were found to decrease for an increasing wave height and current velocity ($\hat{A}_\delta$ = peak orbital amplitude near bed). The angle between the wave and current directions had no significant influence on the ripple dimensions.

The near-bed velocities measured in current-alone conditions (after stopping the wave generator, ripples unchanged) were analyzed by fitting a logarithmic distribution to the measured velocities to determine the physical bed roughness height k_s (Van Rijn 1990). Relatively small k_s-values of 0.5 to 1.5 times the ripple height were found, which might be related to the regular honeycomb ripple pattern. The k_s-values were considerably smaller than those observed earlier (Van Rijn et al. 1993). In this latter flume study with following and opposing current the honeycomb ripple patterns were not observed, but irregular, linguoid (crest ahead of wing tips) three-dimensional ripples were observed.

The reduction of the time-averaged near-bed velocities due to the wave motion effect can be represented by an apparent roughness height k_a (Grant and Madsen 1979; Coffey and Nielsen 1986; Van Rijn 1990). The present data and those of Van Rijn et al. (1993) were analyzed to obtain a functional relationship of the form

$$\frac{k_a}{k_s} = \exp(\gamma \hat{U}_\delta/\bar{u}) \tag{5}$$

in which k_a = apparent roughness height; k_s = physical roughness height; $\hat{U}_\delta$ = peak orbital velocity near the bed, based on linear wave theory and significant wave height and spectral peak period; $\bar{u}$ = depth-averaged current velocity; and γ = empirical coefficient.

The γ-factor was found to be dependent on the wave-current angle: $\gamma = 0.8 + \phi - 0.3\phi^2$, with ϕ in radians between 0 and π. The largest effect in the present tests occurs for a wave current angle of 90° ($\gamma = 1.6$). Eq. (5), which is valid for the rippled bed regime, yields $k_a/k_s = 1$ for $\hat{U}_\delta = 0$ m/s (no wave motion). Eq. (5) is shown in Fig. 7 for three γ-values. More details are given by Van Rijn (1993b).

CURRENT-RELATED SEDIMENT TRANSPORT

Measured Results

The total sediment transport rate ($q_{t,c}$) passing a station is defined as the sum of the suspended-load transport ($q_{s,c}$) and the bed-load transport ($q_{b,c}$). Thus, $q_{t,c} = q_{s,c} + q_{b,c}$ (subscript c refers to current-related transport). The bed-load transport could not be measured in these tests. However, previous tests results show that the bed-load transport is extremely small (Van Rijn et al. 1993). The current-related suspended-load transport is defined as the integration of the product of the time- and space-averaged concentration c_z and velocities u_z from the bed-form crest to the water surface. Thus

$$q_{s,c} = \int_{1/2\Delta}^{h} u_z c_z \, dz \tag{6}$$

First, the current-related transport rate in the main current direction (y) is considered. To estimate the local transport rate in the unmeasured regions between the lowest measuring point and the ripple crest and between the highest measuring point and the water surface, various extrapolation methods were used giving variations of the measured transport rates of about 30% (Van Rijn et al. 1993). This latter value is supposed to be the inaccuracy of the measured suspended-load transport rates. The transport rates are presented in column 3 of Table 2. Analysis of these data showed that the effects of the wave height and current velocity on the transport rate were somewhat smaller than those found earlier by Van Rijn et al. (1993). They found no significant influence of the wave-current angle (following $\phi = 0°$ and opposing $\phi = 180°$) on transport rates. The present data and those of Van Rijn et al. (1993) were combined to a full data set. Analysis of the full data set [see Havinga (1992)] shows a clear influence of the wave-current angle, as presented in Fig. 8. This figure is based on data interpolated from the full data set. The transport rates are maximum for a wave-current angle of 90° which means the waves are propagating normal to the current direction. The reason for this is not fully clear,

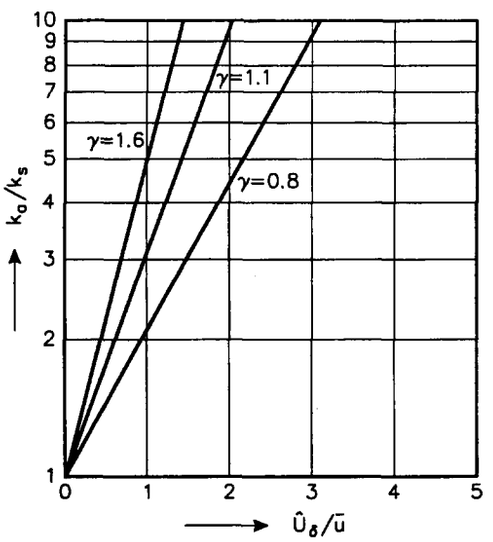

FIG. 7. Ratio of Apparent Roughness and Physical Roughness

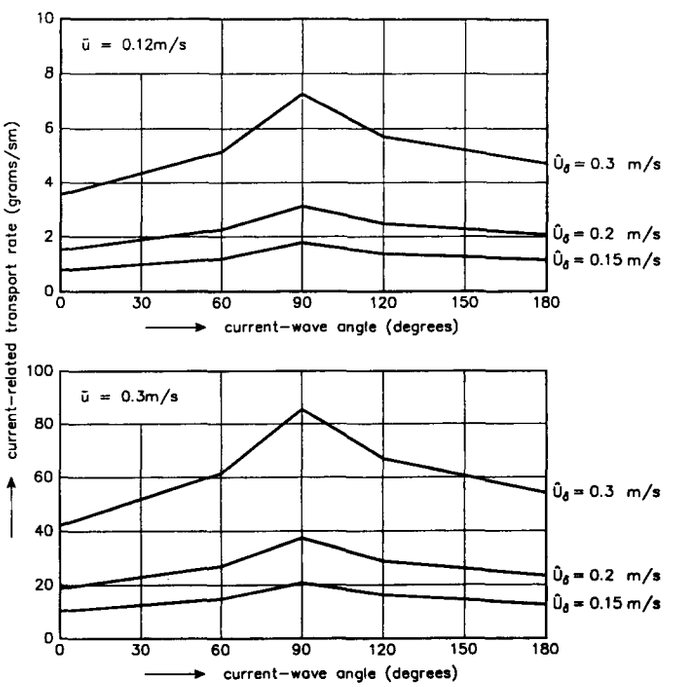

FIG. 8. Transport Rate as Function of Wave-Current Angle

TABLE 2. Sediment Transport Rates Derived from Measured Velocities and Concentrations (Positive x-Direction Is in Wave Direction Onshore, Positive y-Direction Is in Current Direction)

Test code (1)	Depth-Integrated Suspended Load Transport Rates (g/s/m) in Current Direction (y-Direction)				Depth-Integrated Suspended Load Transport Rates (g/s/m) Normal to Current Direction (x-Direction)				Significant Peak Orbital Velocities at Bed (m/s), High-frequency Values	
	Total (2)	Current related (3)	Wave related (high frequency) (4)	Wave related (low frequency) (5)	Total (6)	Current related (7)	Wave related (high frequency) (8)	Wave related (low frequency) (9)	Crest (onshore) (10)	Trough (offshore) (11)
T7 10 90	1.7	1.5	−0.01	0.20	0.22	0.05	0.31	−0.13	0.153	0.133
T7 20 90	6.4	6.3	−0.11	0.22	0.16	0.16	0.09	−0.10	0.155	0.136
T7 30 90	21.9	22.2	−0.21	−0.18	0.62	0.47	0.15	0.01	0.181	0.168
T10 10 90	—	5.3	—	—	—	—	—	—	—	—
T10 20 90	16.9	17.4	−0.25	−0.25	0.57	0.80	0.29	−0.53	0.229	0.200
T10 30 90	38.3	39.1	−0.48	0.33	0.31	0.31	0.49	−0.51	0.224	0.190
T14 10 90	9.8	9.6	−0.03	0.20	−0.28	−0.42	0.59	−0.46	0.277	0.233
T14 20 90	44.3	45.3	−0.54	−0.35	0.86	0.16	1.71	−0.99	0.288	0.216
T14 30 90	71.3	72.9	−0.97	−0.64	2.35	0.32	2.85	−0.82	0.300	0.267
T7 10 90	1.2	0.9	0.04	0.24	−0.13	−0.03	0.01	−0.11	0.120	0.108
T7 20 60	6.3	6.9	−0.48	−0.10	−0.12	0.02	0.04	−0.18	0.154	0.125
T7 30 60	—	30.3	—	—	—	—	—	—	—	—
T10 10 60	—	37.1	—	—	—	—	—	—	—	—
T10 20 60	—	14.2	—	—	—	—	—	—	—	—
T10 30 60	—	31.9	—	—	—	—	—	—	—	—
T14 10 60	—	8.3	—	—	—	—	—	—	—	—
T14 20 60	—	26.1	—	—	—	—	—	—	—	—
T14 30 60	—	49.9	—	—	—	—	—	—	—	—
T7 20 120	—	10.5	—	—	—	—	—	—	—	—
T10 10 120	—	7.7	—	—	—	—	—	—	—	—
T10 20 120	19.0	21.5	−0.40	−0.19	−1.41	−1.29	0.11	−0.24	0.199	0.184
T10 30 120	—	28.1	—	—	—	—	—	—	—	—
T14 10 120	—	8.8	—	—	—	—	—	—	—	—
T14 20 120	—	23.2	—	—	—	—	—	—	—	—
T14 30 120	—	50.4	—	—	—	—	—	—	—	—

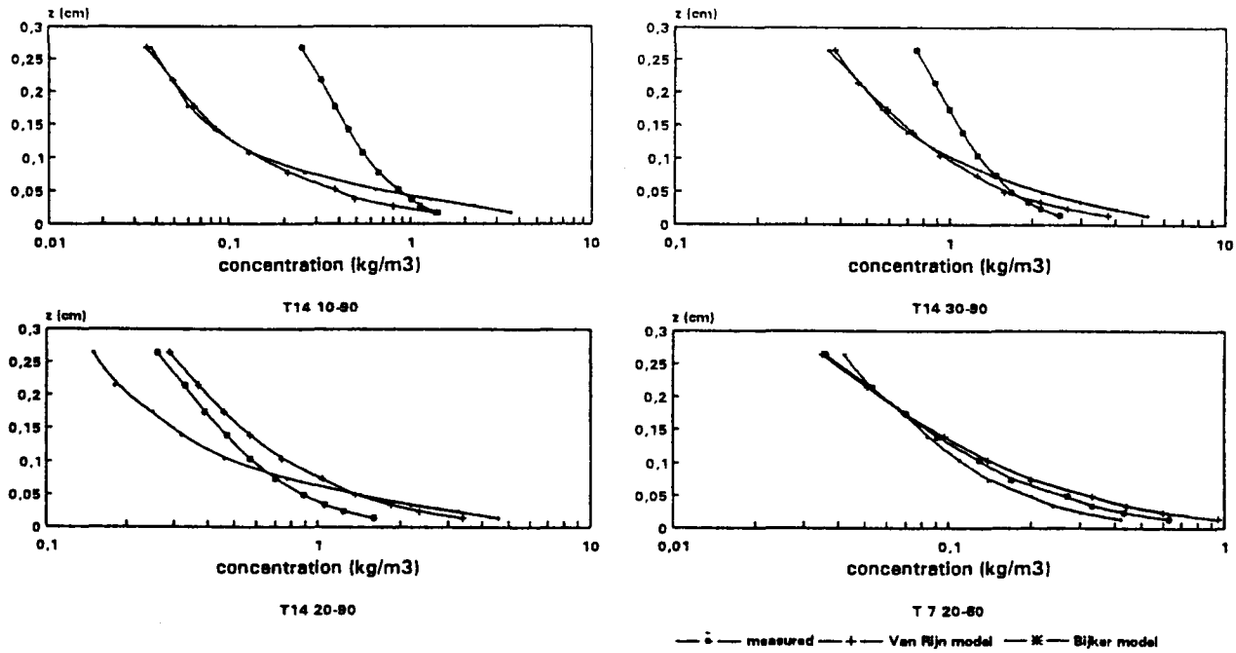

FIG. 9. Measured and Computed Concentration Profiles

but the apparent roughness is also the largest for $\phi = 90°$. This may lead to a larger entrainment rate and mixing effect.

Second, the current-related transport rates in the wave direction (x) are discussed. Instantaneous data were measured in 11 tests. The current-related transport rates in the wave direction (x) were determined by time-averaging the instantaneous data (see column 7 in Table 2). In most tests the current-related transport rate is in the onshore direction. The transport values

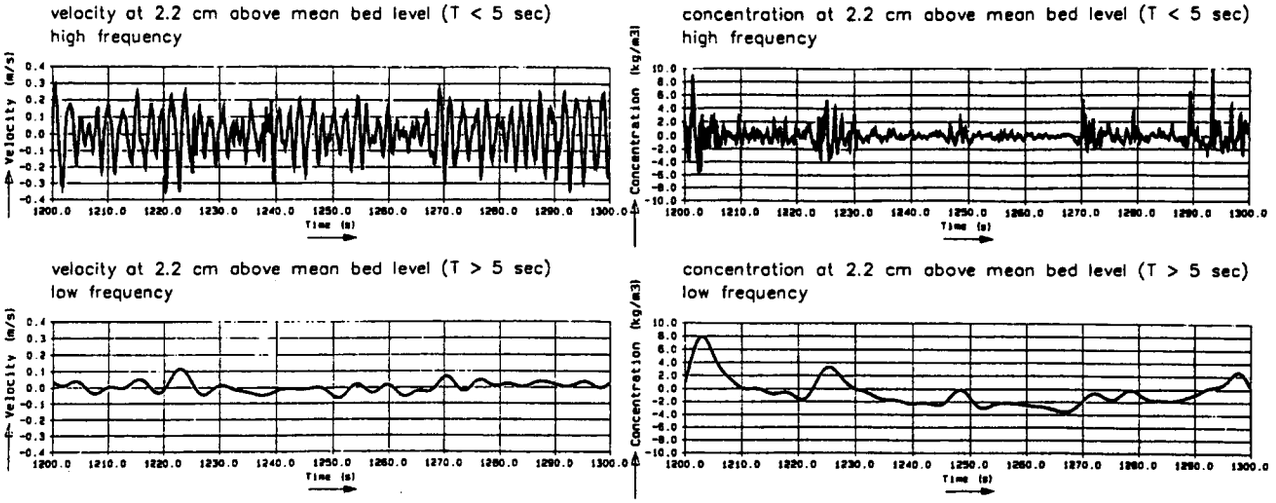

FIG. 10. High-Frequency and Low-Frequency Oscillations and Cross-Shore Velocity and Concentration at z = 0.022 m above Bed, T14.30.90

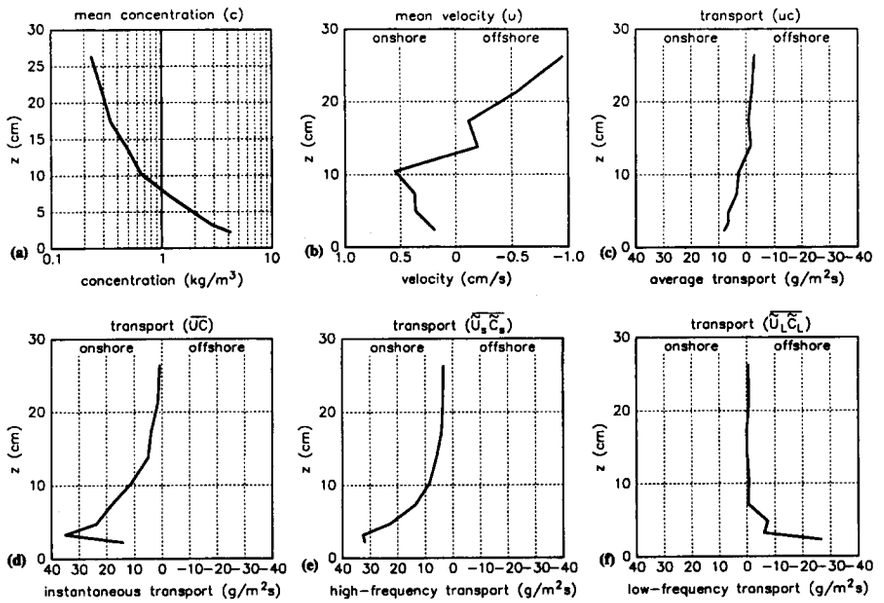

FIG. 11. Vertical Distribution of Mean Concentration, Cross-Shore Velocity, and Transport Rates, T14.30.90

are small because the time-averaged velocities (wave-induced velocities) in the wave direction are small (<0.01 m/s). Although these transport rates are small, they cannot be neglected because their order of magnitude is comparable with those of the other transport components in the wave direction (see columns 6–9, Table 2).

Applied Formulas

The methods of Bijker (1971) and Van Rijn (1985, 1993) were applied to compute the current-related suspended load transport in the main current direction (y) to be compared with the measured transport rates (column 3 in Table 2). Both methods are based on the computation of a time-averaged concentration and velocity profile. The b-coefficient of the Bijker formula, originally proposed to be $b = 5$ (Bijker 1971) for longshore transport, was used as a calibration parameter in this study. A value of $b = 1$ yielded the best overall results. The peak period and significant wave height have been used to represent the wave spectrum (irregular waves) for both methods. Since both methods are sensitive to the bed-roughness parameter (k_s), it was used as a calibration parameter. Van Rijn's method yielded the best results for k_s equals 3 times the ripple height, whereas Bijker's method gave the best results for k_s of about 0.5 times the ripple height. Comparison of measured and computed transport rates showed reasonably good agreement for both methods, similar to results presented by Van Rijn et al. (1993). About 60% of the computed transport rates were within a factor 2 of the measured values.

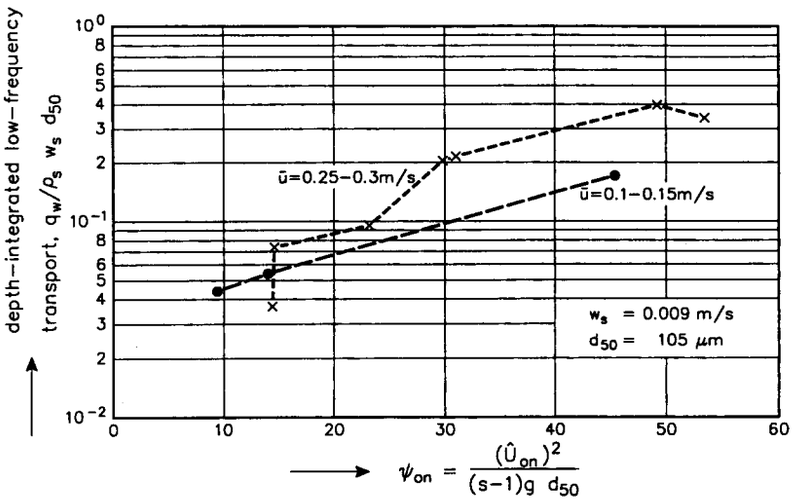

FIG. 12. Low-Frequency Transport

Measured and computed concentration profiles are shown in Fig. 9. Both methods yield reasonable results; Bijker's method overestimates the measured concentrations at low velocities of 0.1 m/s (T14.10.90).

WAVE-RELATED TRANSPORT RATES

To obtain quantitative information on the relative importance of the wave-related transport rate, the available instantaneous velocities and sand concentrations were analyzed using (1)–(4). High- and low-frequency oscillations were separated (by filtering) at a period of 5 s based on spectral analysis. As an example, the instantaneous velocity and concentration data at an elevation of $z = 0.022$ m above the bed for test T14.30.90 are shown in Fig. 10. The low-frequency velocity is offshore-directed under groups of high waves (see t = 1,222, 1,270, and 1,290 s), which are related to the presence of bound long waves (Shi 1983). The high- and low-frequency concentrations are found to be maximum under, and shortly after, relatively high waves.

Fig. 11 shows the vertical distribution of the mean sand concentration, mean cross-shore velocity, and the cross-shore transport rates for the same test. The high-frequency transport component ($\tilde{U}_s\tilde{C}_s$) due to the wave asymmetry effect is directed onshore (normal to the current), whereas the low-frequency transport component ($\bar{U}_L\bar{C}_L$) is directed offshore (bound long wave effect). Both effects are of the same order of magnitude.

The local values above the bed were integrated over the depth. The depth-integrated results are presented in columns 4, 5, 8, and 9 of Table 2. As observed, the wave-related transport rates in the main current direction (y) are small and can be neglected with respect to the current-related transport rate in the y-direction. The wave-related transport rates in the wave direction (x) are also small, but they cannot be neglected because all transport components in the x-direction are of the same order of magnitude.

Analysis of the available data shows consistent and systematic results. The depth-integrated high-frequency transport rates (see Table 2), which are related to the wave asymmetry effect, are onshore-directed in all experiments. The highest transport rates occur for the highest wave conditions. The presence of onshore-directed high-frequency transport rates may be a surprising result, because offshore-directed transport rates were found by others (Sato and Horikawa 1986) in regular waves over a rippled bed. This phenomenon was related to the generation of strong vortex motions in the ripple trough, resulting in phase differences between velocity and concentration peaks. In the present experiments with irregular waves the ripples were not very pronounced, resulting in less significant vortex motions. Ribberink and Al-Salem (1992) also found onshore-directed transport rates in irregular wave conditions over a rippled bed.

The depth-integrated low-frequency transport rates are offshore-directed in nearly all experiments. Fig. 12 shows the dimensionless low-frequency transport rates as a function of a mobility parameter $[(\hat{U}_{on})^2/(s-1)gd_{50}]$, with $\hat{U}_{on}$ = significant peak orbital velocity at bed in the onshore direction (see colums 10 and 11 of Table 2). The low-frequency transport rate increases with increasing peak orbital velocity and mean longshore current velocity ($\bar{u}$).

The most plausible explanation for the presence of offshore-directed low-frequency transport rates is the generation of bound long waves [see, also, Roelvink (1993)]. The slow variation in both the low-frequency concentration and the velocity is the result of the same driving mechanism, and therefore the two are correlated. As a result, the time-averaged value of their product

is nonzero. Such a driving mechanism can be found in the groupiness of the short waves (groups of low and high waves). The groupiness has the following effects: (1) The variations in short-wave energy and associated radiation stresses drive the so-called bound long waves that travel at the group velocity of the short waves; and (2) more sediment is stirred up in groups of high waves than in groups of low waves; a variation in short-wave energy leads to a variation in the concentration of sand.

The covariance between short-wave energy and long-wave velocity is negative if bound waves are the dominant long-wave phenomenon. The covariance between short-wave energy and concentration is positive because the concentration can quickly adapt to changes in short-wave energy. Consequently, the covariance between long-wave velocity and concentration will be negative, resulting in an offshore-directed transport process. Analysis of the instantaneous velocity data showed the proper combination of bound long waves and increased sediment concentrations in groups of high waves (Havinga 1992). As a final conclusion, it is stated that bound long waves have a significant effect on the wave-related transport. In most tests it was of the same order of magnitude as the high-frequency transport rate because of wave asymmetry.

CONCLUSIONS

The generation of waves in the presence of a current caused a decrease of the time-averaged velocities in the near-bed region ($z/h < 0.2$). This effect increased for a larger wave height and was most pronounced for waves propagating normal to the current (rippled bed regime).

A larger wave height leads to larger concentrations and to a steeper (more uniform) concentration profile. A weak current superimposed on the waves moderately affects the concentration profile. A strong current significantly increases concentrations in the near-bed layer and in the upper layer. The concentrations are larger when the waves are propagating in a direction normal to the current.

The physical bed-roughness height was in the range between 0.5 and 1.5 times the ripple height. The current-related suspended load transport in the main current direction (y) was largest for waves propagating normal to the current. Wave-related transport rates in the main current direction were negligible. The comparison of measured and computed current-related transport rates in the longshore direction, based on the methods of Bijker (1971) and Van Rijn (1993) showed reasonable agreement over the full range of conditions. The Bijker method overestimates transport rates at low velocities.

All transport components (mean current effect, high- and low-frequency effects) in the wave direction (normal to the shore) were found to be equally important. Low-frequency transport rates were found to be related to the presence of bound long waves (waves induced by groups of high and low waves).

ACKNOWLEDGMENTS

Jan van de Graaff of Delft University of Technology is gratefully acknowledged for his comments throughout the experimental study.

APPENDIX. REFERENCES

Bijker, E. W. (1971). "Longshore transport computations." *J. Wtrwy., Harb., and Coast., Engrg. Div.*, ASCE, 97(4), 687–703.

Coffey, F. C., and Nielsen, P. (1986). "The influence of waves on current velocity profile." *Coastal Engrg. Conf.*, ASCE, New York, N.Y.

Grant, W. D., and Madsen, O. S. (1979). "Combined wave and current interaction with a rough bottom." *J. Geophysical Res.*, 84(C4), 1797–1808.

Havinga, F. J. (1992). "Sediment concentrations and transport in case of irregular non-breaking waves with a current." *Rep. H840 Parts E, F, G*, Delft Hydr., Delft Univ. of Technol., Delft, The Netherlands.

Kemp, P. H., and Simons, R. R. (1982). "The interaction between waves and a turbulent current: waves propagating with the current." *J. Fluid Mech.*, Vol. 116, 227–251.

Kemp, P. H., and Simons, R. R. (1983). "The interaction between waves and a turbulent current: waves propagating against the current." *J. Fluid Mech.*, Vol. 130, 73–91.

Ribberink, J. S., and Al-Salem, A. (1992). "Time-dependent sediment transport phenomena in oscillatory boundary layer flow under sheet flow conditions." *Rep. H840 Parts IV, V, VI*, Delft Hydr., Delft, The Netherlands.

Roelvink, J. A. (1993). "Surf beat and its effect on cross-shore profiles," PhD dissertation, Delft Univ. of Technology, Delft, The Netherlands.

Sato, S., and Horikawa, K. (1986). "Laboratory studies on sand transport over ripples due to asymmetric oscillatory flows." *Proc., Coast. Engrg. Conf.*, ASCE, New York, N.Y.

Shi, N. C. (1983). "Reverse sediment transport induced by amplitude-modulated waves." *Rep.*, Univ. of Washington, Seattle, Wash.

Van Rijn, L. C. (1985). "Two-dimensional vertical mathematical model for suspended sediment transport by currents and waves." *Rep. S488 part IV*, Delft Hydr., Delft, The Netherlands.

Van Rijn, L. C. (1990). *Principles of fluid flow and surface waves in rivers, estuaries, seas and oceans.* Aqua Publications, Amsterdam, The Netherlands.
Van Rijn, L. C. (1993). *Principles of sediment transport in rivers, estuaries and coastal seas.* Aqua Publications, Amsterdam, The Netherlands.
Van Rijn, L. C. et al. (1993). "Transport of fine sands by currents and waves." *J. Wtrwy. Port, Coast. and Oc. Engrg.*, ASCE, 119(2), 123–143.